



Optimization of Anti-kinking Designs for Vascular Grafts Based on Supramolecular Materials

Dan Jing Wu^{1,2,3}, Kim van Dongen^{1,2,3}, Wojciech Szymczyk^{1,3}, Paul J. Besseling⁴, Ruth M. Cardinaels⁵, Giulia Marchioli^{1,2,3}, Marcel H. P. van Genderen^{1,2}, Carlijn V. C. Bouten^{1,3}, Anthal I. P. M. Smits^{1,3} and Patricia Y. W. Dankers^{1,2,3*}

¹ Institute for Complex Molecular Systems, Eindhoven University of Technology, Eindhoven, Netherlands, ² Laboratory of Chemical Biology, Department of Biomedical Engineering, Eindhoven University of Technology, Eindhoven, Netherlands, ³ Laboratory for Cell and Tissue Engineering, Department of Biomedical Engineering, Eindhoven University of Technology, Eindhoven, Netherlands, ⁴ Department of Nephrology and Hypertension, University Medical Center Utrecht, Utrecht, Netherlands, ⁵ Polymer Technology, Department of Mechanical Engineering, Eindhoven University of Technology, Eindhoven, Netherlands

OPEN ACCESS

Edited by:

Lorenzo Moroni,
Maastricht University, Netherlands

Reviewed by:

Silvia Farè,
Politecnico di Milano, Italy
Fatemeh Kabirian,
Materials and Energy Research
Center, Iran

*Correspondence:

Patricia Y. W. Dankers
P.Y.W.Dankers@tue.nl

Specialty section:

This article was submitted to
Biomaterials,
a section of the journal
Frontiers in Materials

Received: 21 April 2020

Accepted: 15 June 2020

Published: 10 July 2020

Citation:

Wu DJ, van Dongen K,
Szymczyk W, Besseling PJ,
Cardinaels RM, Marchioli G,
van Genderen MHP, Bouten CVC,
Smits AIPM and Dankers PYW (2020)
Optimization of Anti-kinking Designs
for Vascular Grafts Based on
Supramolecular Materials.
Front. Mater. 7:220.
doi: 10.3389/fmats.2020.00220

Synthetic vascular grafts to be applied as access grafts for hemodialysis often require anti-kinking properties. Previously, electrospun microporous vascular implants based on synthetic supramolecular materials have been shown to perform adequately as resorbable grafts due to the microstructures, thereby enabling attraction of endogenous cells and consecutive matrix production *in situ*. Here, we use supramolecular materials based on hydrogen bonding interactions between bisurea (BU) or 2-ureido-4[1H]-pyrimidinones (UPy) to produce microporous anti-kinking tubular structures by combining solution electrospinning with 3D printing. A custom-made rational axis for 3D printing was developed to produce controlled tubular structures with freedom in design in order to print complex tubular architectures without supporting structures. Two different tubular grafts were developed, both composed of a three-layered design with a 3D printed spiral sandwiched in between luminal and adventitial electrospun layers. One tubular scaffold was composed of BU-polycarbonate electrospun layers with 3D printed polycaprolactone (PCL) strands in between for dimensional stability, and the other graft fully consisted of supramolecular polymers, using chain-extended UPy-PCL as electrospun layers and a bifunctional UPy-PCL for 3D printing. Both grafts, with a 3D printed spiral, demonstrated a reproducible dimensional stability and anti-kinking behavior under bending stresses.

Keywords: anti-kinking, graft, supramolecular material, 3D printing, shear-thinning, electrospinning, tubular designs

INTRODUCTION

Kidney patients who depend on hemodialysis require well-functioning vascular access for blood purification. Synthetic vascular grafts are often implanted when patients lack suitable vasculature. However, extensive movement and bending stresses in these grafts can contribute to graft failure (Kannan et al., 2005; De Vries et al., 2016; Pashneh-Tala et al., 2016). For example, the low

stiffness of unstructured vascular grafts causes the lumen to collapse after implantation. When the synthetic grafts are placed a loop configuration, e.g., for vascular access, it is imminent to prevent kinking of the grafts. Nowadays, anti-kinking grafts made from commercial synthetic materials show improved performance using external support from silicone bead structures (Stenoien et al., 1999), plastic rings (Tuchmann and Dinstl, 1989), autologous veins as splints (Agko et al., 2017), or using modified electrospinning collectors to enhance macroscopic anti-kinking structures (Bode et al., 2015). However, these designs may cause complications during vascular surgery procedure, such as clamping and suturing. Moreover, these grafts are often developed from commercial materials such as poly(tetrafluoro ethylene) (PTFE) and poly(ethylene terephthalate) (Dacron). These commercial materials possess major limitations because of a decreased patency rate with increasing implantation time, while the materials should ideally function inside the human body for life (Riepe et al., 1997; Singh et al., 2019). Low patency rates occur owing to multiple factors, such as thrombosis, constrictive remodeling, intimal hyperplasia, infections, and unstable atherosclerotic lesions (Chester, 2002). Therefore, smart graft designs and suitable biomaterials are required in order to adapt to the biological and mechanical conditions of the vascular grafts application, in combination with anti-kinking properties. A relatively new strategy in the vascular replacements is to use bioresorbable scaffolds to fully exploit the regenerative capacity of the body. This approach, also known as the *in situ* tissue engineering approach makes use of cell-free, synthetic, biodegradable scaffolds that provide a temporary instructive environment to support neotissue formation by recruiting the desired cells directly in the functional site of the host (Talacua et al., 2015; Wissing et al., 2017; Smits and Bouten, 2018).

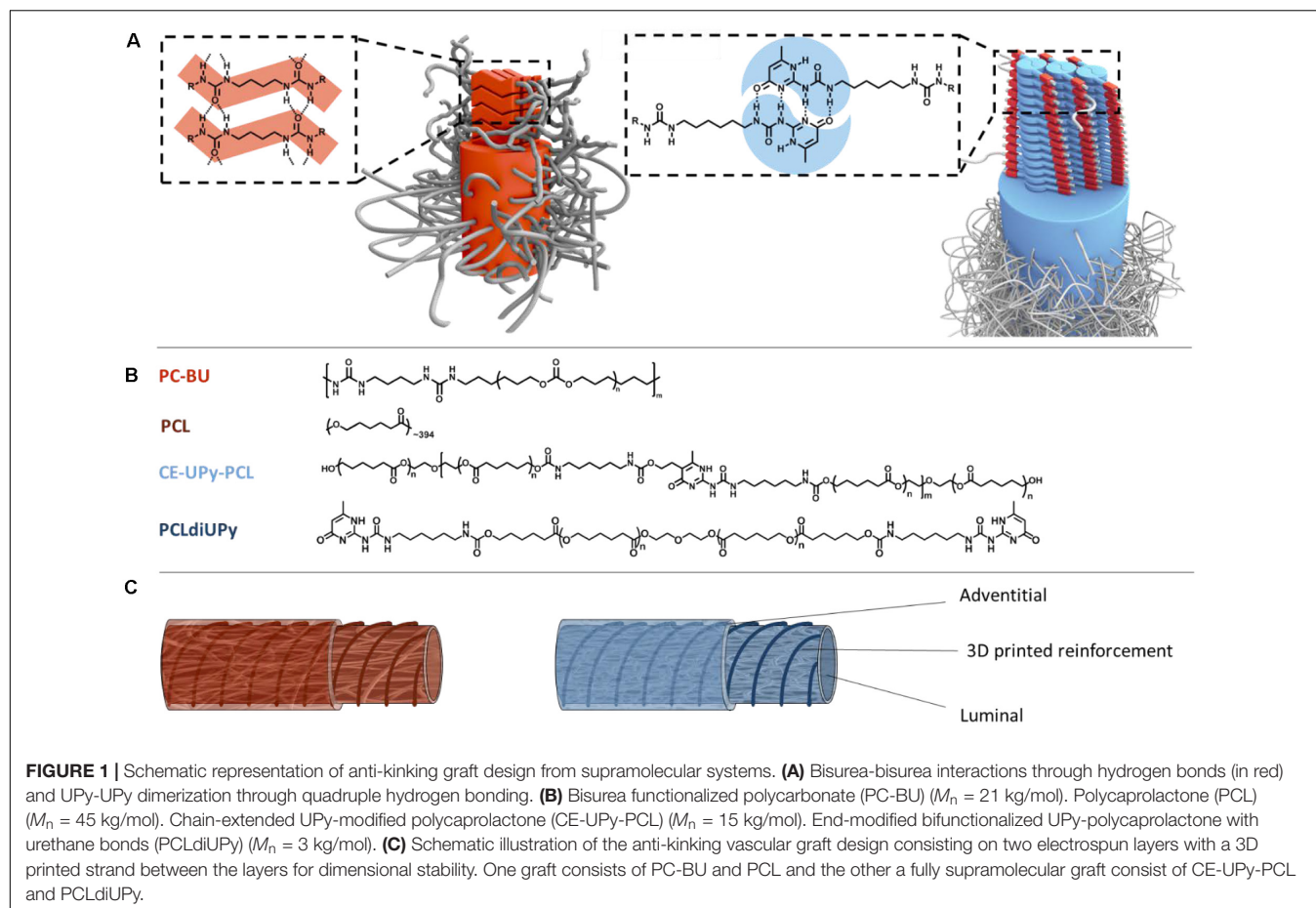
Previously, supramolecular polymers based on bisurea (BU) and 2-ureido-4[1H]-pyrimidinone (UPy)-modified supramolecular polymers were used to develop electrospun microporous vascular grafts that finally are proposed to be biocompatible and fully resorbable (Figure 1A; Van Almen et al., 2016; Kluin et al., 2017; van Haaften et al., 2017; Ippel et al., 2019; van Haaften et al., 2019). These supramolecular polymers have been identified as promising candidates to synthetically mimic the complexity of extracellular matrix (Goor et al., 2017; Diba et al., 2018). Due to their reversible and adaptable nature, the supramolecular materials possess extraordinary mechanical, tunable, responsive and processable properties which cannot be achieved with conventional macromolecules (Aida et al., 2012).

The unique and adaptable mechanical properties of BU-modified polymer arise from the molecular composition, where BU hard-blocks with ability of crystallization through hydrogen-bonding are alternated with a rubbery PC soft-block which ensures biocompatibility and slow degradation (Figure 1B; Appel et al., 2011; van Haaften et al., 2019). The well-defined BU hard-blocks within thermoplastic elastomers enhance the mechanical properties, which is evident from the high tensile strengths (Versteegen et al., 2006). Importantly, we have previously shown that polycarbonate bisurea (PC-BU) enables restoration of endogenous tissue and supports the infiltration of cells and production of extracellular matrix in *in situ* tissue engineered

heart valves and vascular grafts (Brugmans et al., 2015; Kluin et al., 2017). Furthermore, self-complementary UPy-modified thermoplastic elastomers, which can dimerize strongly via quadruple hydrogen bonds, are designed to have load-bearing properties (Sijbesma et al., 1997; Beijer et al., 1998; Dankers et al., 2006; Söntjens et al., 2008). The UPy-modified polymers have previously been developed as bifunctional UPy-polymers in which the UPy-moieties were telechelically coupled to the respective prepolymer (Dankers et al., 2005; Mollet et al., 2014), or as chain-extended UPy-polymers in which the UPy-units are part of the hard block in the main chain of segmented co-polymers (Wisse et al., 2011; Van Almen et al., 2016; Putti et al., 2020). In previous work, biocompatible scaffolds based on different CE-UPy polymers have been applied in *in vivo* vascular graft applications (Muylaert et al., 2016; Van Almen et al., 2016; Bockeria et al., 2017) and have been shown to be mechanical stable, processible and to enhance tissue remodeling, thus support the first steps toward *in situ* tissue engineering (Serruys et al., 2017).

The electrospun microporous supramolecular vascular grafts that we developed previously were implanted in a straight configuration. However, when placement in a loop is needed, e.g., for vascular access, it is imminent to prevent kinking of the grafts. Therefore, here we introduce 3D printing of anti-kinking structures between two electrospun layers (Figure 1C). 3D printing techniques enable vast freedom in development of complex architectures with precise control over specific design properties (Jungst et al., 2015; Wu et al., 2017). In order to produce complex tubular geometries, a custom-built rotary apparatus was developed to enable 3D printing in the rotational axis which enables the production of tubular architectures of any design without printing support structures.

In this study, we use PCL for 3D printing, which is widely used as biomaterial for many 3D printing applications in the field of biomedical engineering (Hutmacher et al., 2001; Brown et al., 2012, 2015). Alternatively, a supramolecular polymer based on oligocaprolactone end-functionalized with UPy-moieties (PCLdiUPy) was used in order to produce a fully supramolecular anti-kinking graft. The luminal (i.e., the inner) layer and the adventitial (i.e., the outer) layer were produced by solution electrospinning, and form a heavily interweaved microfibrillar tubular scaffold (rSupplementary Figure 1). In this way two anti-kinking grafts were designed; one being PC-BU electrospun layers with 3D printed PCL anti-kinking strands, the other being fully supramolecular in nature consisting of CE-UPy-PCL electrospun layers with 3D printed PCLdiUPy anti-kinking strands (Figure 1). First, we investigated the printability of PCL and PCLdiUPy by determining the thermal properties and the rheological properties for extrusion-based 3D printing. Then, the optimization was performed on the 3D printing parameters for the rotational collector in order to control the shape and morphology of anti-kinking designs to enhance reinforcement in synthetic vascular grafts. Finally, the bendability of the grafts was studied using a standardized test method according to the ISO-norms and previous research (Bensch et al., 2016; Brandt-Wunderlich et al., 2016).



EXPERIMENTAL SECTION

Materials

PC-BU ($M_n = 21$ kg/mol) and PCLdiUPy ($M_n = 3$ kg/mol) were synthesized by SyMO-Chem BV (Eindhoven, Netherlands). CE-UPy-PCL ($M_n = 15$ kg/mol) was synthesized by SupraPolix (Eindhoven, Netherlands). PCL ($M_n = 45$ kg/mol) were purchased from Sigma Aldrich (Zwijndrecht, Netherlands).

Differential Scanning Calorimetry

Differential scanning calorimetry (DSC) measurements were performed on a DSC Q2000 (TA instruments, United States). The polymers were weighed, and subsequently hermetically sealed in Tzero aluminum pans. Melting (T_m) and glass (T_g) transition temperatures were measured from the melt, i.e., after the sample had first been brought to the isotropic state, in the second or ensuing heating runs. The samples were subjected to three heating/cooling cycles from -80 to 150°C with a heating/cooling rate of 10 and $40^\circ\text{C}/\text{min}$. The data was analyzed and quantified using Universal Analysis software (V4.5A, TA Instruments).

Rheology

Films were prepared by compression molding. Discs of 8 mm diameter were prepared by punching. Rotational viscosity

experiments were performed on an Anton Paar Physica MCR-501 rheometer (Anton Paar GmbH, Germany). Parallel plates with a plat-plate geometry of 50 mm and gap distance of 1 mm were used. All measurements were performed under a nitrogen atmosphere to prevent thermo-oxidative degradation at 150°C with a shear rate between 0.01 and 100 s^{-1} . To estimate the true shear rate first the shear thinning behavior was described by using the power law model (Dantzig and Tucker, 2001):

$$\eta = m\dot{\gamma}^{n-1}$$

Thermogravimetric Analysis

Measurements were performed on a Perkin-Elmer TGA 7 using the high-resolution dynamic mode, from room temperature to 400°C at a heating rate of $10^\circ\text{C}/\text{min}$. Samples were placed in platinum pans, and experiments were performed under an atmosphere of air (flow rate 20 mL/min).

Electrospinning Equipment

Electrospinning solutions were prepared by dissolving the polymer in organic solvent at room temperature and stirring overnight. Electrospinning was performed on equipment of IME 14 Technologies EC-CLI (IME Technologies, Waalre, Netherlands). A 6 mm collector drum was used, pre-coated with a 2% solution of alginic acid sodium salt from brown algae

in ultra-pure water. Mandrels were coated and left in a 37°C incubator for 5 min. This is repeated once and followed by an incubation step of 30 min.

Electrospinning Parameters

Bisurea-based grafts: an electrospinning solution was prepared consisting of 22 wt% of PC-BU in chloroform (CHCl₃)/hexafluoro-2-propanol (HFIP) 85:15. A voltage of 17 kV was applied on the electrospinning nozzle and negatively charge (−1 kV) on the rotating collector (ø 6 mm) and −3 kV for the second layer. Flow rate was set on 70 µL per minute and chloroform vapor in the gas shield module set at 35 mL/min to stabilize the electrospinning jet. Temperature was set on 23°C and relative humidity on 50%. The base layer of each sample was electrospun for 27 min and top layer for 7 min, with a fiber uptake speed of 0.09 m/s. Nozzle speed was 10 mm/s, tip-collector distance 15.5 cm and polymer solution was fed through a needle with an inner diameter of 0.8 mm. A turn delay was used for 1,000 ms on both ends.

UPy-based grafts: an electrospinning solution was prepared of 22 wt% of CE-UPy-PCL in HFIP. Applied voltage was 15 kV on the electrospinning nozzle and a negatively charge (−1 kV) on the rotating collector (ø 6 mm) and −3 kV for the second layer. Flow rate was set on 40 µL per minute and nozzle speed was set on 7 mm/s. The polymer solution was fed through a needle with an inner diameter of 0.8 mm. Temperature was 23°C and relative humidity 30%. The first electrospun layer had a spinning time of 65 min and the second layer of 12 min, with a fiber uptake speed of 0.13 m/s. Tip-collector distance was set at 19 cm for the base layer and 17 cm for the second layer. Turn delay was set on 1,500 ms on both ends.

3D Printing Reinforced Architectures

Fused deposition modeling (FDM) 3D printing (Biobot 1, Philadelphia, PA, United States) was used to produce the reinforced architectures. A Standard Triangle Language (STL-) file was created using a CAD software (SketchUp, Denver, CO, United States) and with RepetierHost converted into a g-code. X-axis speed was a variable in the transcript and extrusion rate was set to 0.54 mm/s. A custom made rotatory collector has been for printing of tubular architectures (**Supplementary Figure 2**). The collector distance between the printing nozzle (25 G; d_I = 260 µm) was calibrated to 5 mm. PCLdiUPy or PCL was loaded and molten at 120°C into a metal syringe and stabilized for 15 min before printing. The printing of the material was performed using pressure of 80 PSI.

Next, the flow rate Q was obtained using the flow of a power law fluid in a tube (represents the printing nozzle) (Dantzig and Tucker, 2001):

$$Q = \int_0^{2\pi} \int_0^R v_{\zeta}(r) r dr d\theta = \frac{\pi}{s+3} \left(\frac{\Delta p}{2mL} \right)^s R^{s+3}$$

With $v_{\zeta}(r)$ the velocity, L the length of the nozzle, R its diameter and Δp the pressure drop, s equals $1/n$.

The true shear rate at the wall within the printer nozzle was obtained from Morrison (2001):

$$\dot{\gamma}_R = - \left. \frac{dv_{\zeta}}{dr} \right|_{r=R} = \left(\frac{4Q}{\pi R^3} \right) \left(\frac{\frac{1}{n} + 3}{4} \right)$$

The calculated value is the maximum value due to the consideration of a shear rate distribution from zero in the center of the tube to maximum at the wall. Furthermore, this calculation takes the pressure drop in the printing nozzle into account (this effect in the printing nozzle is dominant), it neglects pressure drop in the printing reservoir and the converging flow from the reservoir toward the printing nozzle. The polymer melt was printed on a 6 mm diameter rotational mandrel with various nozzle speeds (between 0.1 and 11 mm/s). Quantification of fiber diameter, spacing and angles were done with a Keyence VHX-500FE digital microscope prior to electrospinning the second layer and scaffold removal from the mandrel.

Removal of Anti-kinking Vascular Graft From Mandrel

Electrospun grafts were placed in the vacuum oven overnight at 37°C. Subsequently, they were placed in a bottle with demineralized water and stored in −30°C overnight. The grafts were then subjected to thawing at room temperature and the electrospinning mandrel was gently removed after 40 min. After complete removal of ice, scaffolds were dried at room temperature for at least 24 h and placed in the vacuum oven for at least 2 h.

Microstructure Characterization

The scaffold microstructures were characterized with scanning electron microscopy (SEM; Quanta 600F, Fei, Hillsboro, OR, United States). Samples were cut in liquid nitrogen prior to imaging and PC-BU scaffolds were treated with gold sputter-coating. Images were taken in high vacuum atmosphere at 2 kV and spot size 3 nm. The fiber diameter and pore size were quantified using software of ImageJ (U.S. National Institutes of Health, Bethesda, MD, United States). Fiber diameter was quantified by measuring at 24 different positions. Pore size was quantified by manual thresholding of the images, followed by skeletonizing.

Bending Test

Bending tests were performed on an in-house-created set-up, which is developed according to ISO 7198:8:9. The bending radius was measured with a digital caliper for each vascular graft with 6 mm in diameter and a total length of 10 cm. The lumen loss of the examined graft while bent around the respective radius was calculated according to: $\Delta D = 100\% \times (D_0 - D_i)/D_0$, with D_0 as the diameter of the graft in original configuration and D_i as diameter at the respective bending radius. The testing was performed under atmospheric condition and room temperature.

RESULTS

Material Printability

In general, polymers for 3D printing must fulfill a number of key requirements for processing with an extrusion-based 3D printer, such as appropriate melting temperature, degradation temperature, and viscosity of the material. To address the printability, these properties of two selected polymers, PCL and PCLdiUPy, were characterized to gain information that is relevant for the 3D printing process. First, differential scanning calorimetry (DSC) measurements were performed to study the thermal behavior of the polymers and to determine the polymer melting temperature (Table 1 and Figure 2A). For PCL, the DSC thermograph shows a glass transition (T_g) at -61°C with a single melting peak (T_m) at 55°C (Figure 2A). Moreover, an expected phase-separated morphology was observed for PCLdiUPy with two melting transitions. The first melting transition (T_{m1}) of 38°C is from the semi-crystalline PCL soft block and a second melting transition (T_{m2}) of 81°C is related to the UPy-urethane-moieties forming the hard block.

Thermogravimetric analysis (TGA) was performed to confirm the decay temperature of the polymers to ensure a sufficient thermal stability during 3D printing since it requires melting of the polymer for extrusion and material deposition. The decay temperatures (T_{decay}) at 5% weight loss are determined by TGA for PCL at 331.9°C and PCLdiUPy at 275.1°C (Table 1 and Figure 2B). This observation demonstrates no weight loss in all the materials below the decay temperature. Hence, the biomaterials are thermally stable during the 3D printing process with the determined melting temperatures using DSC (Table 1).

The viscosity of PCL and PCLdiUPy was analyzed in the range of shear rates that is representative for the extrusion process during 3D printing (Figure 2C). The low viscosity of PCL is independent of the shear rate, therefore a Newtonian rheological behavior is observed. This means that the material will flow whereby the flow rate will increase proportionally with the applied pressure. In contrast, the viscosity of PCLdiUPy demonstrates a non-Newtonian rheological behavior, which is shear rate dependent. The decrease of the viscosity with increasing shear rates indicates that the material is shear-thinning. This can be explained by the hydrogen-bonds of the UPy-modified polymers, which can break at high temperatures ($T > T_m$) and shear rates, resulting in flexible polymer chains (Xu et al., 2011). This phenomenon can be beneficial for 3D printing in general; as pressure is applied for polymer extrusion, shear stresses will be generated in the nozzle for polymer extrusion. Moreover, a maximum shear rate of $1.4 \times 10^7 \text{ s}^{-1}$ was calculated using rheological models described in the experimental section

for PCLdiUPy, which is based on the flow of a fluid in a tube. This apparent high shear rate confirms that the shear thinning of PCLdiUPy is relevant for the extrusion-based 3D printing technique. Therefore, supramolecular polymers with shear-thinning behavior are promising candidates for 3D printing, as their resistance to flow will decrease with increasing pressure drops. In conclusion, based on these results, PCL and PCLdiUPy are thermally stable at the melting temperature and both materials are able to flow during printing extrusion.

Designing 3D Printed Tubular Architectures

The dimensional stability of the tubular graft can be manipulated by introducing 3D printed architectures between the luminal and adventitial electrospun layers to reinforce the lumen. With the variation of the architectural design, tubular grafts can resist deformation during bending stresses (Connolly et al., 2015), including axial extension, radial expansion and twisting. For 3D printing, a custom-made rotating cylindrical collector was developed to replace the traditional static printing collector in order to print complex tubular architectures in an rotational axis without supporting structures, which enables additional degree of freedom in 3D printing (Supplementary Figure 2). Optimization is required in order to develop a dimensionally stable and reinforced design to enhance anti-kinking of the vascular graft. To determine the kink resistance for vascular grafts in a standardized manner, a custom made bending apparatus with a 4–30 mm bending radius (Supplementary Figure 3) was developed in order to determine the kinking at bending stresses.

Tubular Cross-Pattern, Ring and Spiral Designs

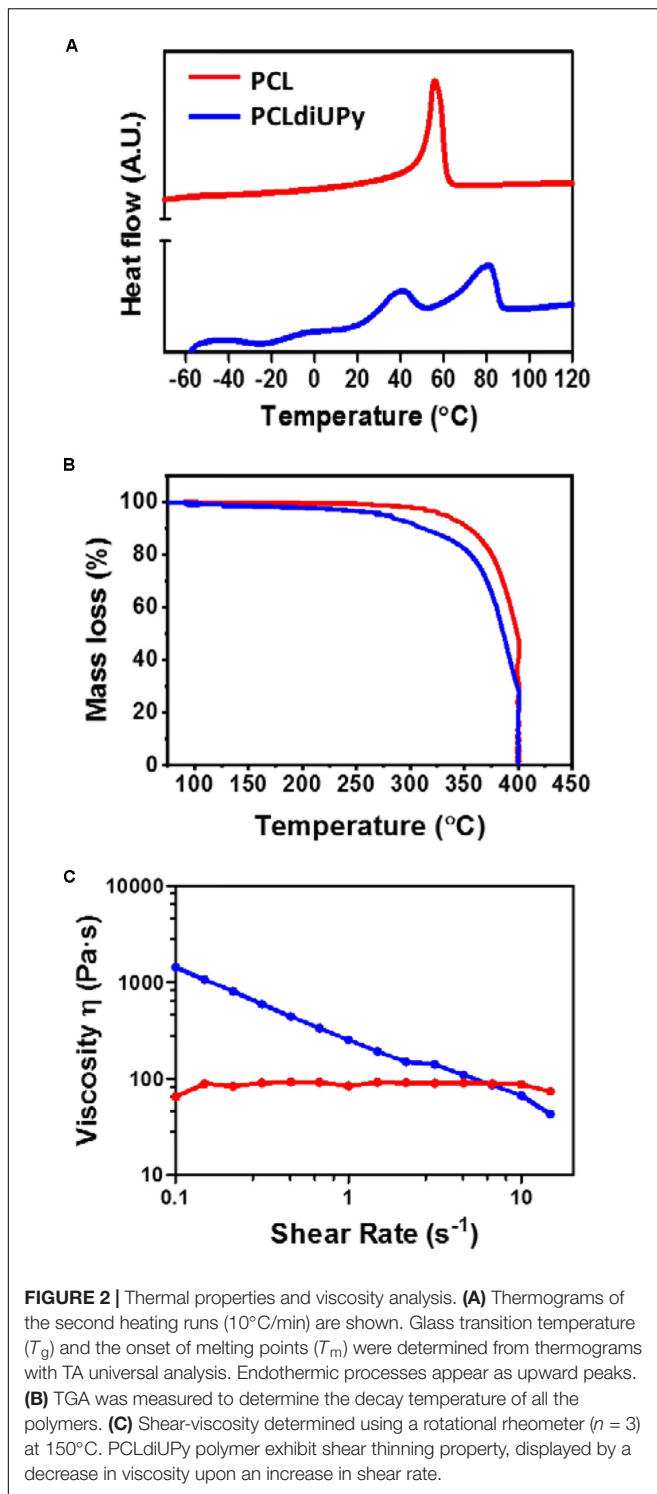
The grafts with various 3D printed tubular patterns have been designed and studied with a custom-made bending apparatus (Figure 3). Firstly, pristine electrospun microporous PC-BU and CE-UPy-PCL tubular scaffolds were fabricated and both grafts displayed kinking already at all bending radii (4–30 mm) with more than 50% diameter reduction (Figures 3A,H,K).

Subsequently, three types of 3D printed tubular designs were tested, namely a cross-pattern, a ring and a spiral design. A cross-pattern design was introduced with a printed spacing of $7,100 \pm 61 \mu\text{m}$, fiber thickness of $150 \pm 11 \mu\text{m}$ and angle of 74° (Figure 3B). Unfortunately, this graft displayed kinking of the lumen at the intersection of the printed crossing strands. The cross pattern has large open space between the repeating pattern (next to the crossing position) which results in a weak point within the grafts and therefore kinking of the graft was observed (Figure 3B). Hence, the cross-pattern design was not further optimized or used for further studies. Ring

TABLE 1 | Thermal properties of PCL and PCLdiUPy.

	M_n (kg/mol)	T_g ($^\circ\text{C}$)	$T_{m,1}$ ($^\circ\text{C}$)	$\Delta H_{m,1}$ (J/g)	$T_{m,2}$ ($^\circ\text{C}$)	$\Delta H_{m,2}$ (J/g)	T_{decay}^* ($^\circ\text{C}$)
PCL	4.5	-61	55	69.8	-	-	331.9
PCLdiUPy	3.0	-55	38	70.7	81	71.6	275.1

Values of the second heating runs ($10^\circ\text{C}/\text{min}$) are shown. The following variables are shown: the average molecular weight (M_n), the glass transition temperature (T_g), the melting peaks ($T_{m,1}$ and $T_{m,2}$) the heat fusion ($\Delta H_{m,1}$ and $\Delta H_{m,2}$), the degradation temperature (T_{decay}). * Determined at 5% weight loss.



design (90°) was developed for both materials: PC-BU graft with PCL rings thickness of $645 \pm 25 \mu\text{m}$ and $2,344 \pm 515 \mu\text{m}$ spacing (Figure 3C) and CE-UPy-PCL graft with PCLdiUPy rings thickness of $860 \pm 60 \mu\text{m}$ and $2,093 \pm 84 \mu\text{m}$ spacing (Figure 3I). The ring design prevents gross luminal collapse of the graft with less than 50% diameter reduction of the

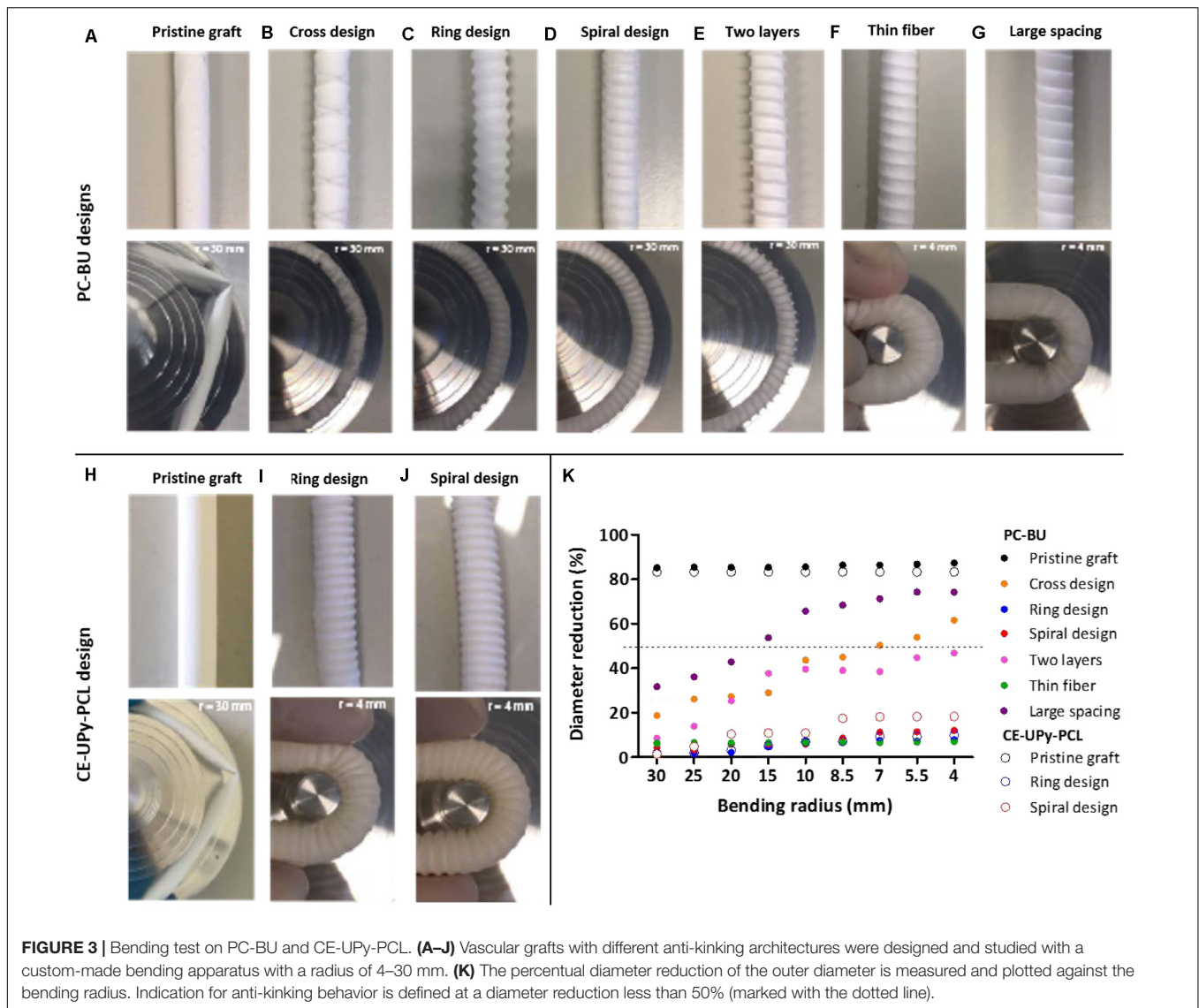
lumen during bending (Figure 3K). However, minimal local kinking in between the rings was visually observed. The ring design is intrinsically a dimensionally less stable entity due to the lack of interconnected architecture between the printed structures. Finally, a spiral design was produced with a PCL strand thickness of $709 \pm 9.0 \mu\text{m}$, $2,434 \pm 75 \mu\text{m}$ spacing and angle of 84° (Figure 3D). For PCLdiUPy strand, a spiral thickness of $1,030 \pm 18 \mu\text{m}$, $1,898 \pm 33 \mu\text{m}$ spacing and an 83° angle was produced (Figure 3J). The spiral design displayed local kinking resistance and dimensional stability in the lumen no occurrence of folds was observed. The spiral design showed promising results with good anti-kinking properties for the BU- and UPy-based grafts.

Optimization of Spiral Architectures

Having established the superior anti-kinking properties of the spiral design, we proceeded to optimize the parameters of the printed spiral graft design. In order to study the influence of the second electrospun layer on anti-kinking properties, a spiral-reinforced graft without the adventitial layer produced and tested (Figure 3E). Apparent kinking of the lumen was observed when decreasing in bending radius, which indicates dimensional instability without the adventitial electrospun layer of the vascular graft. Next, a graft with an adjusted thickness of the 3D printed strand was developed. The reinforcement in this graft had approximately half of the fiber thickness, with a thickness of $358 \pm 30 \mu\text{m}$, spacing $2,679 \pm 50 \mu\text{m}$ and angle of 83° (Figure 3F). A decreased fiber diameter was achieved by significantly decreasing the printing pressure, due to less material deposition on the rotational mandrel. Using semi-quantitative analysis, dimensional stability in the lumen of the graft was observed, even up to the minimum bending radius of 4 mm (Figure 3F). Additionally, 3D printed spirals were developed with larger spacing to explore the limits of dimensional stability (Figure 3G). Grafts with an increased spiral spacing of $2,729 \pm 120 \mu\text{m}$ was developed. Interestingly, a diameter reduction in the lumen was observed for this graft up to a bending radius of 4 mm (Figure 3H). These results provide an indication for the range of parameters (strand spacing and thickness) in order to develop an optimal design for anti-kinking grafts (Figure 3K).

Systematic Optimization of 3D Printed Spiral Design

The spiral design is interconnected between the luminal and adventitial layers, which provides dimensional stability during bending. However, the spiral architectures can be influenced by many factors such as mandrel rotation and nozzle deposition speed. These are critical factors that can influence the diameter, the spacing and the angle of the printed strands with respect to the vascular graft (Sodupe-Ortega et al., 2018). Therefore, a systematic study was set up to explore the variety of the parameters. The change in the nozzle speed and rotational mandrel velocity resulted in the development of a highly controlled continuous strand with a variety of reproducible spacing, fiber thickness and fiber angle (Figure 4). The nozzle speed in the X-axis, from 0.1 to 1 mm/s,



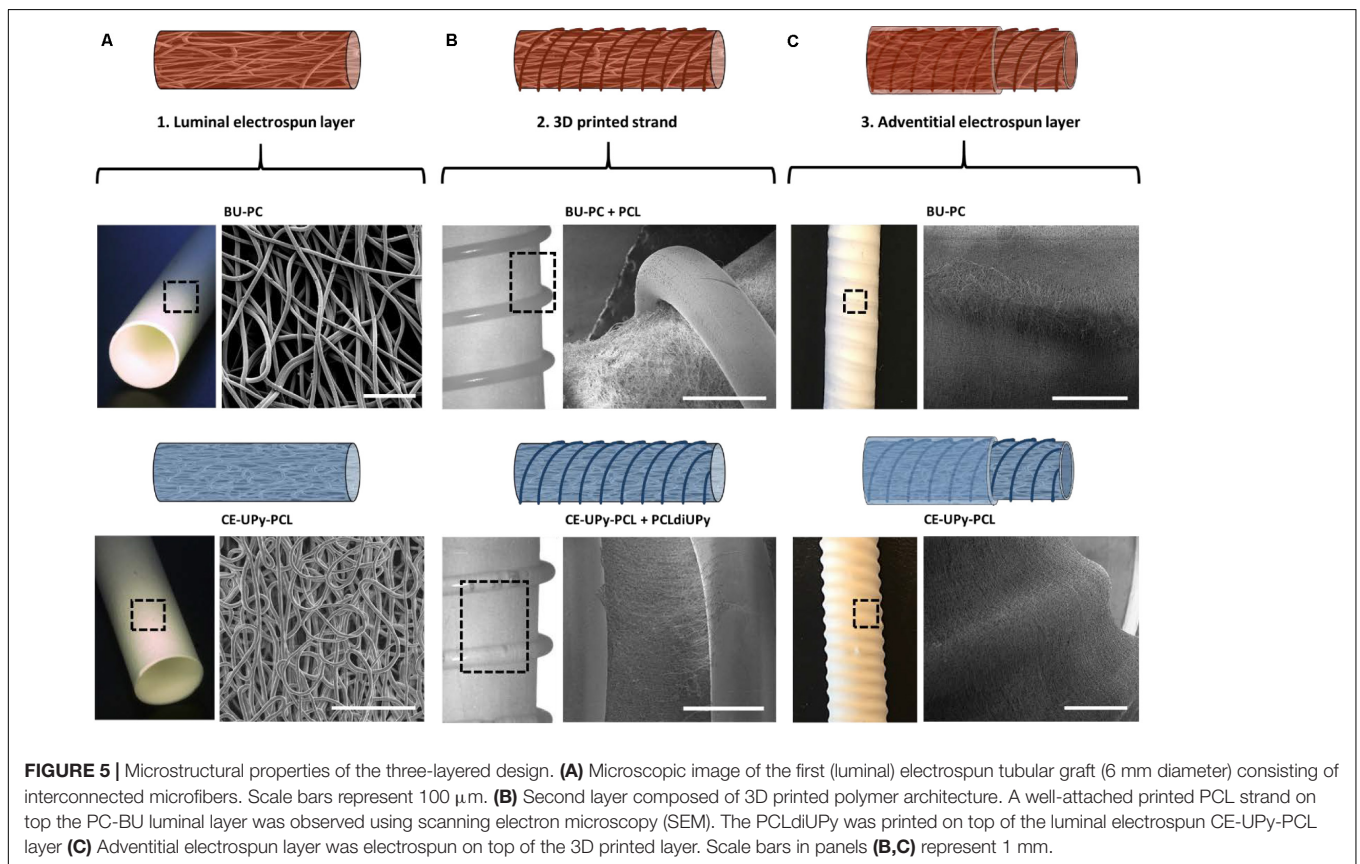
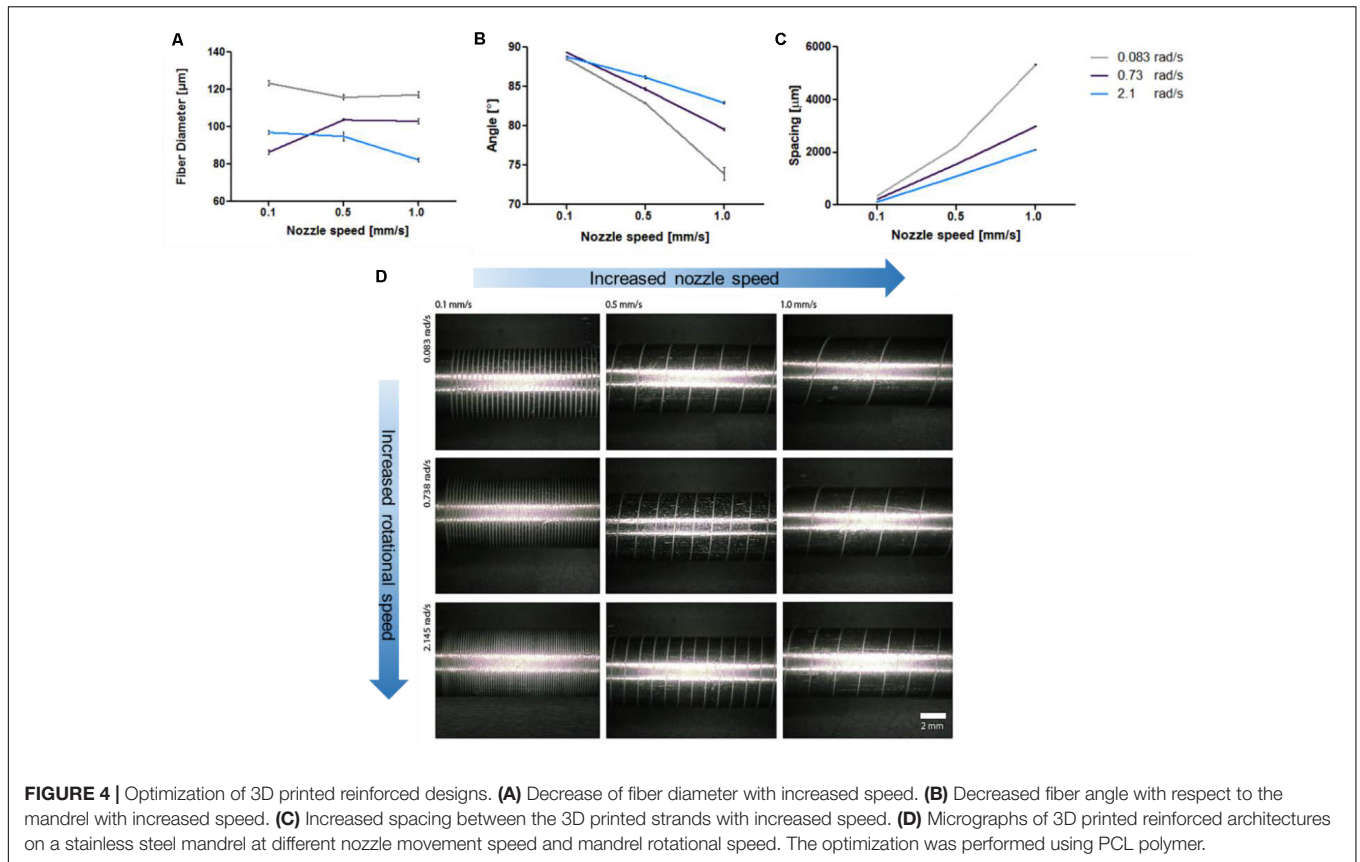
was tested in combination with rotational speed from 0.083 to 2.1 rad/s. In addition, increased nozzle speed (1–9 mm/s) were studied in combination with increased rotational speed (**Supplementary Figure 4**). However, these results did not demonstrate reproducible thickness of the printed strand ranging from 15 to 175 μm due to the increased speed. The increase of the printing velocity in the nozzle and rotational speed resulted in less controlled and poorly reproducible architectures. Therefore, the low nozzle speed (0.1–1 mm/s) and low rotational speed (0.083–2.1 rad/s) were used to produce 3D printed reinforced architectures with reproducible results.

As the pressure during printing might influence the result, the printing pressure was kept constant at 80 PSI in order to extrude the polymer melt. In general, the increase of the nozzle speed resulted in a slight decrease of the fiber diameter for most rotational velocities (Žarko et al., 2017). Interestingly, a decrease in angle degree and increase of spacing size was observed upon increasing of the nozzle speed (**Figure 4**). An

increased nozzle speed in the X-axis results in faster material deposition. Furthermore, the change in speed of the rotational movement showed to influence the architecture design as well. Specifically, an increase in rotational velocity progressively led to a decrease in fiber diameter and fiber spacing, as well as an increase in fiber angle. These effects were most pronounced at higher nozzle speeds.

Morphology Analysis of the Anti-kinking Graft

The luminal electrospun layer with an internal diameter of 6 mm was produced from either PC-BU or CE-UPy-PCL polymers. Importantly, SEM micrographs showed non-fused interconnected microfibers in the luminal and adventitial electrospun layers, demonstrating a dense porous network with an average fiber diameter of $3.6 \pm 0.35 \mu\text{m}$ for the PC-BU grafts and $3.0 \pm 0.66 \mu\text{m}$ in the CE-UPy-PCL grafts (**Figure 5A**).



The PC-BU graft consist of a luminal electrospun layer of $511 \pm 74 \mu\text{m}$ and an adventitial layer of $261 \pm 33 \mu\text{m}$. The CE-UPy-PCL graft consists of a luminal wall of $504 \pm 36 \mu\text{m}$ and an adventitial layer of $260 \pm 17 \mu\text{m}$. The 3D printed reinforced structure was sandwiched between the luminal and adventitial electrospun layer (**Figure 5B**). No morphological changes have been observed after 3D printing on top of the electrospun layer. Moreover, good attachment of the electrospun layers was observed via electron micrograph of the cross section of the grafts (**Supplementary Figure 5**). Finally, the adventitial layer either from PC-BU or CE-UPy-PCL was electrospun on top of the 3D printed strand to support the dimensional change and provide minimal change in the wall of the grafts (**Figure 5C**).

DISCUSSION AND CONCLUSION

Previous *in situ* tissue engineering studies have shown that synthetic grafts based on supramolecular materials are able to perform as regenerative resorbable grafts, which enable attraction of endogenous cells and consecutive matrix production *in situ* (Talacua et al., 2015; Muylaert et al., 2016; Van Almen et al., 2016; van Haaften et al., 2019). However, kinking in the flexible lumen, as well as changes in the wall are complications that cause low patency of the vascular grafts. In this study, we optimized the anti-kinking properties of supramolecular tubular grafts using 3D printing of a continuous strand to reinforce the lumen. In previous work, promising BU-PC and CE-UPy-PCL polymers have been used to develop flexible vascular grafts and heart valves for *in vivo* applications (Brugmans et al., 2015; Muylaert et al., 2016; Van Almen et al., 2016; Bockeria et al., 2017; Kluin et al., 2017). However, kinking in the flexible lumen (of approximately $700 \mu\text{m}$ thickness) has been observed when the grafts were placed in a loop configuration (**Figures 3A,H**). In general, the lumen of commercial grafts (Dacron) and many other vascular grafts are consisting of a thickness range between 400 and $700 \mu\text{m}$ (Stanley et al., 1982; Rothuizen et al., 2016). Therefore, Lee et al. studied mechanical enhancement in tubular structures using an efficient dual 3D processing technique by developing two-layered vascular grafts based on electrospinning of a natural polymer, chitosan with poor mechanical properties, fully coated with polycaprolactone (PCL) for reinforcement (Lee et al., 2015). Albeit resulting in enhanced mechanical properties, this design may restrict graft bending due to the complete coverage with PCL, which might limit the surgical approach during implantation. Therefore, the structural design of the tubular architecture is important in order to provide dimensional stability without restriction in bending flexibility of the vascular grafts. Here, we showed the efficiency to provide dimensional stability by developing an interconnected architecture sandwiched between the luminal and adventitial electrospun layers to prevent kinking of the lumen but remain flexibility. Various designs of stable 3D printed architectures were explored by varying printing velocity, i.e., nozzle speed, in combination with a rotating collector. This study showed enhanced dimensional stability of supramolecular vascular grafts under bending stress by improving the design

with a three-layered approach. Despite the different material properties, this design has shown to be effective for anti-kinking behavior in both supramolecular BU- and UPy-systems. PC-BU grafts contains a PCL reinforced strand, which could lead to different degradation rates since PCL crystallization is not based on hydrogen bonding. In contrast, a fully UPy-based vascular graft consists of two polymers with comparable components in molecular design and based on hydrogen bonding.

In conclusion, using a 3D printed spiral as reinforcement between the lumen of two electrospun layers showed to be the optimal anti-kinking design for both bisurea and UPy-polymer grafts. Pristine electrospun grafts displayed kinking with more than 50% diameter reduction. Subsequently, three types of 3D printed anti-kinking designs were tested, namely a cross-pattern, a ring and a spiral design. The spiral design demonstrates effective anti-kinking behavior when the graft was placed in a loop configuration. Importantly, a fully supramolecular graft with anti-kinking properties was made from UPy-modified polymers used in the electrospun layers and for the 3D printing of the spiral, which demonstrates the broad possibilities of using UPy-polymers for different purposes and processing methods (i.e., electrospinning and 3D printing).

DATA AVAILABILITY STATEMENT

The raw data supporting the conclusions of this article will be made available by the authors, without undue reservation.

AUTHOR CONTRIBUTIONS

DW, KD, GM, and PD conceived and designed the experiments. DW, KD, and WS performed the analysis. PB, RC, CB, AS, PD, and MG analyzed data. All authors contributed to manuscript revision, read and approved the submitted version.

FUNDING

This work was funded by the Ministry of Education, Culture and Science (Gravity Program 024.001.03) and ZonMW as part of the LSH 2Treat program (Project No. 436001003).

ACKNOWLEDGMENTS

The authors thank R. Anastasio for the useful discussions on the results, A.M.A.O Pollet for the technical support during some of the 3D printing experiments, and A.W. Bosman (SupraPolix) for providing the CE-UPy-PCL polymer.

SUPPLEMENTARY MATERIAL

The Supplementary Material for this article can be found online at: <https://www.frontiersin.org/articles/10.3389/fmats.2020.00220/full#supplementary-material>

REFERENCES

- Agko, M., Liu, E., Huang, T. C. T., Lo Torto, F., Ciudad, P., Manrique, O. J., et al. (2017). The split vein graft "splint" to avoid kinking and compression of the vascular pedicle. *Microsurgery* 37, 739–740. doi: 10.1002/micr.30179
- Aida, T., Meijer, E. W., and Stupp, S. I. (2012). Functional supramolecular polymers. *Science* 335, 813–817. doi: 10.1126/science.1205962
- Appel, W. P. J., Portale, G., Wisse, E., Dankers, P. Y. W., and Meijer, E. W. (2011). Aggregation of ureido-pyrimidinone supramolecular thermoplastic elastomers into nanofibers: a kinetic analysis. *Macromolecules* 44, 6776–6784. doi: 10.1021/ma201303s
- Beijer, F. H., Sijbesma, R. P., Kooijman, H., Spek, A. L., and Meijer, E. W. (1998). Strong dimerization of ureidopyrimidones via quadruple hydrogen bonding. *J. Am. Chem. Soc.* 120, 6761–6769. doi: 10.1021/ja974112a
- Bensch, M., Müller, M., Bode, M., and Glasmacher, B. (2016). Automation of a test bench for accessing the bendability of electrospun vascular grafts. *Curr. Dir. Biomed. Eng.* 2, 307–310. doi: 10.1515/cdbme-2016-0068
- Bockeria, L. A., Svanidze, O., Kim, A., Shatalov, K., Makarenko, V., Cox, M., et al. (2017). Total cavopulmonary connection with a new bioabsorbable vascular graft: first clinical experience. *J. Thorac. Cardiovasc. Surg.* 153, 1542–1550. doi: 10.1016/j.jtcvs.2016.11.071
- Bode, M., Mueller, M., Zernetsch, H., and Glasmacher, B. (2015). Electrospun vascular grafts with anti-kinking properties. *Curr. Dir. Biomed. Eng.* 1:125. doi: 10.1515/cdbme-2015-0125
- Brandt-Wunderlich, C., Schwerdt, C., Behrens, P., Grabow, N., Schmitz, K.-P., and Schmidt, W. (2016). A method to determine the kink resistance of stents and stent delivery systems according to international standards. *Curr. Dir. Biomed. Eng.* 2, 289–292. doi: 10.1515/cdbme-2016-0064
- Brown, T. D., Edin, F., Datta, N., Skelton, A. D., Huttmacher, D. W., and Dalton, P. D. (2015). Melt electrospinning of poly(ϵ -caprolactone) scaffolds: phenomenological observations associated with collection and direct writing. *Mater. Sci. Eng. C* 45, 698–708. doi: 10.1016/j.msec.2014.07.034
- Brown, T. D., Slotoch, A., Thibaudeau, L., Taubenberger, A., Loessner, D., Vaquette, C., et al. (2012). Design and fabrication of tubular scaffolds via direct writing in a melt electrospinning mode. *Biointerphases* 7, 1–16. doi: 10.1007/s13758-011-0013-7
- Brugmans, M. C. P., Söntjens, S. H. M., Cox, M. A. J., Nandakumar, A., Bosman, A. W., Mes, T., et al. (2015). Hydrolytic and oxidative degradation of electrospun supramolecular biomaterials: in vitro degradation pathways. *Acta Biomater.* 27, 21–31. doi: 10.1016/j.actbio.2015.08.034
- Chester, J. F. (2002). The causes of synthetic vascular graft failure. *Ann. Coll. Surg. Hong Kong* 6, 97–101. doi: 10.1046/j.1442-2034.2002.00149.x
- Connolly, F., Polygerinos, P., Walsh, C. J., and Bertoldi, K. (2015). Mechanical programming of soft actuators by varying fiber angle. *Soft Robot.* 2, 26–32. doi: 10.1089/soro.2015.0001
- Dankers, P. Y. W., Harmsen, M. C., Brouwer, L. A., Van Luyn, M. J. A., and Meijer, E. W. (2005). A modular and supramolecular approach to bioactive scaffolds for tissue engineering. *Nat. Mater.* 4, 568–574. doi: 10.1038/nmat1418
- Dankers, P. Y. W., van Leeuwen, E. N. M., van Gemert, G. M. L., Spiering, A. J. H., Harmsen, M. C., Brouwer, L. A., et al. (2006). Chemical and biological properties of supramolecular polymer systems based on oligocaprolactones. *Biomaterials* 27, 5490–5501. doi: 10.1016/j.biomaterials.2006.07.011
- Dantzig, J. A., and Tucker, C. L. (2001). *Modeling in Materials Processing*. Cambridge: Cambridge university press.
- De Vries, M. R., Simons, K. H., Jukema, J. W., Braun, J., and Quax, P. H. A. (2016). Vein graft failure: from pathophysiology to clinical outcomes. *Nat. Rev. Cardiol.* 13, 451–470. doi: 10.1038/nrcardio.2016.76
- Diba, M., Spaans, S., Ning, K., Ippel, B. D., Yang, F., Loomans, B., et al. (2018). Self-healing biomaterials: from molecular concepts to clinical applications. *Adv. Mater. Interfaces* 5, 1–21. doi: 10.1002/admi.201800118
- Goor, O. J. G. M., Keizer, H. M., Bruinen, A. L., Schmitz, M. G. J., Versteegen, R. M., Janssen, H. M., et al. (2017). Efficient functionalization of additives at supramolecular material surfaces. *Adv. Mater.* 29:1604652. doi: 10.1002/adma.201604652
- Huttmacher, D. W., Schantz, T., Zein, I., Ng, K. W., Teoh, S. H., and Tan, K. C. (2001). Mechanical properties and cell cultural response of polycaprolactone scaffolds designed and fabricated via fused deposition modeling. *J. Biomed. Mater. Res.* 55, 203–216. doi: 10.1002/1097-4636(200105)55:2<203::AID-JBM1007<3.0.CO;2-7
- Ippel, B. D., Keizer, H. M., and Dankers, P. Y. W. (2019). Supramolecular antifouling additives for robust and efficient functionalization of elastomeric materials. *Mol. Design Matter.* 29:1805375. doi: 10.1002/adfm.201805375
- Jungst, T., Muerza-Cascante, M. L., Brown, T. D., Standfest, M., Huttmacher, D. W., Groll, J., et al. (2015). Melt electrospinning onto cylinders: effects of rotational velocity and collector diameter on morphology of tubular structures. *Polym. Int.* 64, 1086–1095. doi: 10.1002/pi.4948
- Kannan, R. Y., Salacinski, H. J., Butler, P. E., Hamilton, G., and Seifalian, A. M. (2005). Current status of prosthetic bypass grafts: a review. *J. Biomed. Mater. Res. Part B Appl. Biomater.* 74, 570–581. doi: 10.1002/jbm.b.30247
- Kluin, J., Talacua, H., Smits, A. I. P. M., Emmert, M. Y., Brugmans, M. C. P., Fioretta, E. S., et al. (2017). In situ heart valve tissue engineering using a bioresorbable elastomeric implant – from material design to 12 months follow-up in sheep. *Biomaterials* 125, 101–117. doi: 10.1016/j.biomaterials.2017.02.007
- Lee, S. J., Heo, D. N., Park, J. S., Kwon, S. K., Lee, J. H., Lee, J. H., et al. (2015). Characterization and preparation of bio-tubular scaffolds for fabricating artificial vascular grafts by combining electrospinning and a 3D printing system. *Phys. Chem. Chem. Phys.* 17, 2996–2999. doi: 10.1039/C4CP04801F
- Mollet, B. B., Comellas-Aragonès, M., Spiering, A. J. H., Söntjens, S. H. M., Meijer, E. W., and Dankers, P. Y. W. (2014). A modular approach to easily processable supramolecular bilayered scaffolds with tailorable properties. *J. Mater. Chem. B* 2, 2483–2493. doi: 10.1039/c3tb21516d
- Morrison, F. A. (2001). *Understanding Rheology*. Oxford: Oxford University Press.
- Muylaert, D. E. P., van Almen, G. C., Talacua, H., Fledderus, J. O., Kluin, J., Hendrikse, S. I. S., et al. (2016). Early in-situ cellularization of a supramolecular vascular graft is modified by synthetic stromal cell-derived factor-1 α derived peptides. *Biomaterials* 76, 187–195. doi: 10.1016/j.biomaterials.2015.10.052
- Pashneh-Tala, S., MacNeil, S., and Claeysens, F. (2016). The tissue-engineered vascular graft - Past, present, and future. *Tissue Eng. Part B Rev.* 22, 68–100. doi: 10.1089/ten.teb.2015.0100
- Putti, M., Mes, T., Huang, J., Bosman, A. W., and Dankers, P. Y. W. (2020). Multi-component supramolecular fibers with elastomeric properties and controlled drug release. *Biomater. Sci.* 8, 163–173. doi: 10.1039/c9bm01241a
- Riepe, G., Loos, J., Imig, H., Schroder, A., Schneider, E., Petermann, J., et al. (1997). Long-term in vivo alterations of polyester vascular grafts in humans. *Eur. J. Vasc. Endovasc. Surg.* 13, 540–548. doi: 10.1016/S1078-5884(97)80062-7
- Rothuizen, T. C., Damanik, F. F. R., Lavrijsen, T., Visser, M. J. T., Hamming, J. F., Lalai, R. A., et al. (2016). Development and evaluation of in vivo tissue engineered blood vessels in a porcine model. *Biomaterials* 75, 82–90. doi: 10.1016/j.biomaterials.2015.10.023
- Serruys, P. W., Miyazaki, Y., Katsikis, A., Abdelghani, M., Leon, M. B., Virmani, R., et al. (2017). Restorative valve therapy by endogenous tissue restoration: tomorrow's world? Reflection on the EuroPCR 2017 session on endogenous tissue restoration. *EuroIntervention* 13, AA68-AA77. doi: 10.4244/EIJ-D-17-00509
- Sijbesma, R. P., Beijer, F. H., Brunsveld, L., Folmer, B. J. B., Hirschberg, J. H. K. K., Lange, R. F. M., et al. (1997). Reversible polymers formed from self-complementary monomers using quadruple hydrogen bonding. *Science* 278, 1601–1604. doi: 10.1126/science.278.5343.1601
- Singh, G., Cordero, J., Wiles, B., Tembelis, M. N., Liang, K.-L., Rafailovich, M., et al. (2019). Development of in vitro bioengineered vascular grafts for microsurgery and vascular surgery applications. *Plast. Reconstr. Surg. Glob. Open* 7:e2264. doi: 10.1097/gox.0000000000002264
- Smits, A. I. P. M., and Bouten, C. V. C. (2018). Tissue engineering meets immunoengineering: prospective on personalized in situ tissue engineering strategies. *Curr. Opin. Biomed. Eng.* 6, 17–26. doi: 10.1016/j.cobme.2018.02.006
- Sodupe-Ortega, E., Sanz-Garcia, A., Pernia-Espinoza, A., and Escobedo-Lucea, C. (2018). Accurate calibration in multi-material 3D bioprinting for tissue engineering. *Materials (Basel)* 11:1402. doi: 10.3390/ma11081402
- Söntjens, S. H. M., Renken, R. A. E., Van Gemert, G. M. L., Engels, T. A. P., Bosman, A. W., Janssen, H. M., et al. (2008). Thermoplastic elastomers based on strong and well-defined hydrogen-bonding interactions. *Macromolecules* 41, 5703–5708. doi: 10.1021/ma800744c
- Stanley, J. C., Burkel, W. E., Ford, J. W., Vinter, D. W., Kahn, R. H., Whitehouse, W. M., et al. (1982). Enhanced patency of small-diameter, externally supported

- Dacron iliofemoral grafts seeded with endothelial cells. *Surgery* 92, 994–1005. doi: 10.5555/uri:pii:0039606082901611
- Stenoien, M. D., Drasler, W. J., Scott, R. J., and Jenson, M. L. (1999). *Silicone Composite Vascular Graft*. Google Patents. Washington, DC: U.S. Patent and Trademark Office.
- Talacua, H., Smits, A. I. P. M., Muylaert, D. E. P., Van Rijswijk, J. W., Vink, A., Verhaar, M. C., et al. (2015). In situ tissue engineering of functional small-diameter blood vessels by host circulating cells only. *Tissue Eng. Part A* 21, 2583–2594. doi: 10.1089/ten.tea.2015.0066
- Tuchmann, A., and Dinstl, K. (1989). Below-knee femoropopliteal bypass using externally supported polytetrafluoroethylene (PTFE) grafts. *Ann. Vasc. Surg.* 3, 177–180. doi: 10.1016/S0890-5096(06)62013-X
- Van Almen, G. C., Talacua, H., Ippel, B. D., Mollet, B. B., Ramaekers, M., Simonet, M., et al. (2016). Development of non-cell adhesive vascular grafts using supramolecular building blocks. *Macromol. Biosci.* 16, 350–362. doi: 10.1002/mabi.201500278
- van Haften, E., Bouten, C., and Kurniawan, N. (2017). Vascular mechanobiology: towards control of in situ regeneration. *Cells* 6:19. doi: 10.3390/cells6030019
- van Haften, E. E., Duijvelshoff, R., Ippel, B. D., Söntjens, S. H. M., van Houtem, M. H. C. J., Janssen, H. M., et al. (2019). The degradation and performance of electrospun supramolecular vascular scaffolds examined upon in vitro enzymatic exposure. *Acta Biomater.* 92, 48–59. doi: 10.1016/j.actbio.2019.05.037
- Versteegen, R. M., Kleppinger, R., Sijbesma, R. P., and Meijer, E. W. (2006). Properties and morphology of segmented copoly(ether urea)s with uniform hard segments. *Macromolecules* 39, 772–783. doi: 10.1021/ma051874e
- Wisse, E., Spiering, A. J. H., Dankers, P. Y. W., Mezari, B., Magusin, P. C. M. M., and Meijer, E. W. (2011). Multicomponent supramolecular thermoplastic elastomer with peptide-modified nanofibers. *J. Polym. Sci. Part A Polym. Chem.* 49, 1764–1771. doi: 10.1002/pola.24598
- Wissing, T. B., Bonito, V., Bouten, C. V. C., and Smits, A. I. P. M. (2017). Biomaterial-driven in situ cardiovascular tissue engineering—a multi-disciplinary perspective. *NPJ Regen. Med.* 2, 1–19. doi: 10.1038/s41536-017-0023-2
- Wu, D. J., Bouten, C. V. C., and Dankers, P. Y. W. (2017). From molecular design to 3D printed life-like materials with unprecedented properties. *Curr. Opin. Biomed. Eng.* 2, 43–48. doi: 10.1016/j.cobme.2017.06.001
- Xu, D., Liu, C.-Y., and Craig, S. L. (2011). Divergent shear thinning and shear thickening behavior of supramolecular polymer networks in semidilute entangled polymer solutions. *Macromolecules* 44, 2343–2353. doi: 10.1021/acs.chemrev.5b00303
- Žarko, J., Vladiaè, G., Pál, M., and Dedijer, S. (2017). Influence of printing speed on production of embossing tools using FDM 3d printing technology. *J. Graph. Eng. Des.* 8, 19–27. doi: 10.24867/jged-2017-1-019

Conflict of Interest: The authors declare that the research was conducted in the absence of any commercial or financial relationships that could be construed as a potential conflict of interest.

Copyright © 2020 Wu, van Dongen, Szymczyk, Besseling, Cardinaels, Marchioli, van Genderen, Bouten, Smits and Dankers. This is an open-access article distributed under the terms of the Creative Commons Attribution License (CC BY). The use, distribution or reproduction in other forums is permitted, provided the original author(s) and the copyright owner(s) are credited and that the original publication in this journal is cited, in accordance with accepted academic practice. No use, distribution or reproduction is permitted which does not comply with these terms.